OVERVIEW OF HEAVY IONS FROM THE ATLAS EXPERIMENT*

Helena Santos

on behalf of the ATLAS Collaboration

LIP — Laboratório de Instrumentação e Física Experimental de Partículas
Av. Gama Pinto, 2, 1649-003 Lisboa, Portugal

(Received March 26, 2019)

The experimental data collected by the ATLAS experiment during the LHC Run 2 provide a broad physics program to probe and characterize the Quark–Gluon Plasma created in these collision systems. The large acceptance and high granularity of the detector is well-suited to perform detailed analyses on bulk phenomena, electroweak probes, quarkonia, charged particles and jets. In these proceedings, the latest results on these observables will be described, including comparisons with those produced in lighter p+Pb and pp collisions, as well as with theoretical predictions.

DOI:10.5506/APhysPolB.50.1217

1. Introduction

A wide research program is ongoing at the Large Hadron Collider with the aim of studying the properties of Quantum Chromodynamics at extreme conditions. Ultra-relativistic heavy-ion collision data suggest that matter subject to extreme conditions of temperature and density undergoes a phase transition from an ordinary hadronic phase to a plasma of quarks and gluons, the QGP. The Heavy Ion Program of the LHC in Run 2 used lead beams colliding at the centre-of-mass energy of 2.76 TeV and 5.02 TeV and xenon beams colliding at 5.44 TeV. Proton–lead collisions at $\sqrt{s_{NN}} = 5.02$ TeV and 8.16 TeV took also place and play a crucial role in the program as the results contribute to the understanding of cold nuclear matter effects. Such effects are also expected to be present in reactions of heavier nuclei, but they are difficult to disentangle from those originating from the QGP. Proton–proton collisions at $\sqrt{s} = 2.76$ TeV and 5.02 TeV were also provided and constitute a valuable reference for modifications of the observables in heavier collision systems with respect to those in vacuum. ATLAS [1] has shown an excellent

* Presented at the Cracow Epiphany Conference on Advances in Heavy Ion Physics, Kraków, Poland, January 8–11 2019.

performance through Run 2. The large acceptance and high granularity of the ATLAS detector is well-suited to study the phenomena occurring in heavy-ion collisions. In order to estimate the collision centrality, the total transverse energy deposited in the forward calorimeters, FCal ($\sum E_{\mathrm{T}}^{\mathrm{FCal}}$ in $3.2 \leq |\eta| < 4.9$), is used and compared to a Glauber Monte Carlo model [2], convoluted with pp data taken at the same beam energy. The $\sum E_{\mathrm{T}}^{\mathrm{FCal}}$ distribution is then divided into percentiles of the total inelastic cross section for Pb+Pb (or Xe+Xe) collisions. The nuclear thickness function, $\langle T_{AA} \rangle$, and number of participants in a collision, N_{part}, for each centrality interval are also estimated using the Glauber model [3].

2. Flow

An observable that gives insight into the earliest phase of the collisions is the elliptic flow, which arises when two colliding nuclei do not overlap completely. In such a case, the initial-spatial anisotropy leads to a final-state elliptical asymmetry in the momentum space with respect to the reaction plane defined by the impact parameter and the beam axis. The observed anisotropy is characterised as a Fourier series

$$\frac{\mathrm{d}N}{\mathrm{d}\phi} \equiv \frac{N_0}{2\pi} \left(1 + 2 \sum_{n=1}^{\infty} v_n \cos\left(n \left(\phi - \Phi_n \right) \right) \right) ,$$

where ϕ is the azimuthal angle of the particle momentum, and the harmonics v_n and phases Φ_n are the magnitude and phase of the n^{th}-order anisotropy. The v_n coefficients are typically functions of p_{T}, η and particle species, and are referred to as flow-harmonics, while the Φ_n are referred to as event-plane angles. In ATLAS, these planes are estimated using the FCal. The "elliptic flow" parameter v_2 is the second Fourier coefficient. Higher order components of the Fourier decomposition, having their respective reaction planes, are expected to be induced by initial event-by-event fluctuations. The different v_n parameters are measured using tracks in the Inner Detector ($|\eta| < 2.5$). "Non-flow" contributions are minimized by maximizing the gap between the track and the reaction plane, that is, by using the reaction plane estimated in the opposite FCal hemisphere relative to the measured track [3].

The interest of studying flow in Xe+Xe collisions is two-fold. The xenon nucleus is smaller than the lead nucleus and this implies larger event-by-event fluctuations leading to larger eccentricities in the initial geometry. On the other hand, a smaller system implies larger viscous effects of the hydrodynamic expansion [4]. It is important to check if hydrodynamics, that successfully describes the flow in lead–lead collisions, still describes the flow in xenon–xenon interactions. The magnitude of the harmonics flow,

v_n, increases from central to peripheral collisions, peaking around 30–40% centrality [5]. The ratios of the coefficients v_n, measured in the two collision systems through the 2-particle correlations method (2PC) [5], are shown in Fig. 1 and concern the integrated p_{T} interval of the second particle from 0.5 to 5 GeV [1], as the analysis reveals a weak dependence on p_{T}. Each column corresponds to a different n. The magnitude of the ratios for v_2 decreases with decreasing collision centrality becoming negative by 10–15% centrality. The value of coefficient v_3 in xenon–xenon values is larger than in lead–lead over the 0–30% centrality interval. These observations are well in agreement with hydrodynamic predictions [4]. See Ref. [5] for analysis details.

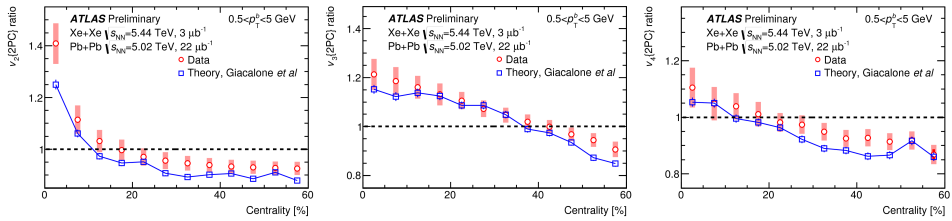

Fig. 1. (Colour on-line) Ratios of the Xe+Xe v_n to the Pb+Pb v_n, concerning the 0.5–5 GeV p_{T} interval. From left to right, v_n measurements are reported for $n = 2$, 3 and 4. The ratios are compared to theoretical predictions computed in the 0.3–5 GeV p_{T} interval from Ref. [4]. The error bars and bands indicate statistical and systematic uncertainties, respectively. See Ref. [5].

3. γ–jet correlations

A suitable observable to probe jet energy loss is the jet energy relative to photon energy, as photons do not experience the strong interaction and will emerge untouched from the fireball. The transverse momentum and pseudorapidity cuts applied to photons in the current analysis are $63.1 < p_{\mathrm{T}}^{\gamma} < 200$ GeV and $|\eta_{\gamma}| < 2.37$, while for jets are $p_{\mathrm{T}}^{\mathrm{jet}} > 31.6$ GeV and $|\eta_{\mathrm{jet}}| < 2.8$. The transverse momentum balance given by the jet-to-photon p_{T} ratio, $x_{\mathrm{J}\gamma}$, is measured for pairs with azimuthal opening angle $\Delta\phi > 7\pi/8$. Figure 2 shows the distributions of the per-photon jet yield as a function of $x_{\mathrm{J}\gamma}$, $(1/N_{\gamma})(\mathrm{d}N/x_{\mathrm{J}\gamma})$, fully corrected for detector effects using a two-dimensional unfolding procedure and reported at the particle level. The top set of plots concerns the p_{T} of the photon in the 63.1–79.6 GeV range and the bottom set concerns the 100–158 GeV p_{T} range. Whereas there is a pp-like peaked $x_{\mathrm{J}\gamma}$, independently of jet p_{T} in peripheral Pb+Pb, a striking structure evolving with collision centrality and sensitive to jet p_{T} is observed. Noticeable is the increasing double peak, interpreted as resulting from parton energy loss in the hot nuclear medium [6].

[1] ATLAS uses natural units, where $c = 1$.

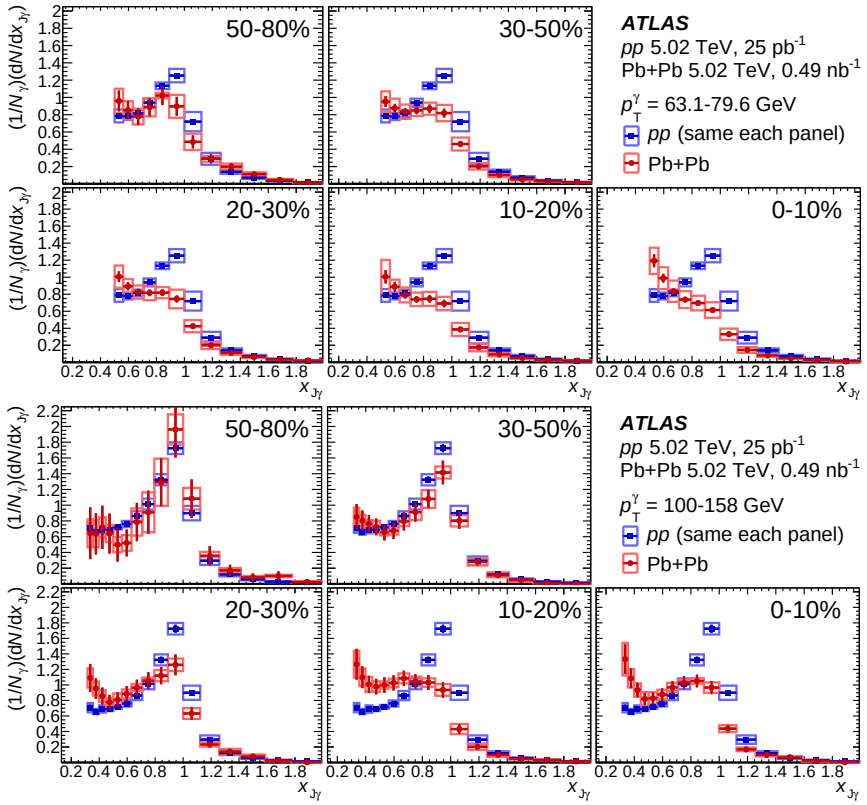

Fig. 2. (Colour on-line) Fully unfolded and corrected photon-jet p_{T}-balance distributions, $(1/N_\gamma)(\mathrm{d}N/x_{\mathrm{J}\gamma})$, in Pb+Pb events (red circles) with each panel showing a different centrality selection compared to that in pp events (blue squares). Total systematic uncertainties are shown as boxes, while statistical uncertainties are shown as vertical bars. Top: results for $p_{\mathrm{T}}^{\gamma} = 63.1$–$79.6$ GeV. Bottom: results for $p_{\mathrm{T}}^{\gamma} = 100$–$158$ GeV [6].

4. Dimuons in non-ultra-peripheral collisions via $\gamma\gamma$ scattering

Dimuon pairs resulting from the intense magnetic fields produced by the lead ions, occurring simultaneously with the hadronic collisions, have been analysed. Events are selected by a trigger requiring at least two muons, each having transverse momentum $p_{\mathrm{T}} > 4$ GeV. Events are further required to have a reconstructed primary vertex, built from at least two tracks with $p_{\mathrm{T}} > 0.4$ GeV. At analysis level, each muon is required to have $p_{\mathrm{T}} > 4$ GeV and $|\eta| < 2.4$. An invariant mass requirement of $4 < m_{\mu^+\mu^-} < 45$ GeV is applied to suppress the contribution from hadron (primarily J/ψ meson) decays and Z-boson decays to muon pairs. Dimuon distributions are corrected

for trigger and reconstruction inefficiencies. Results are shown in Fig. 3. Although the dimuons are balanced in transverse momentum through the asymmetry variable, $A = (p_{\mathrm{T}}{}^{+} - p_{\mathrm{T}}{}^{-})/(p_{\mathrm{T}}{}^{+} + p_{\mathrm{T}}{}^{-})$, their acoplanarity, defined as $\alpha = 1 - |\phi^{+} - \phi^{-}|/\pi$, is increasingly broadened with the collision centrality. Background from dimuons resulting from heavy-flavour decays is estimated with a template fit method and subtracted. Background associated to the Drell–Yan pairs and $\Upsilon(nS)$ mesons is found to be negligible in the phase space of the measurement. The STARlight model [7] predicts the behaviour in peripheral collisions but not in central. However, it should be stressed that, due to the intrinsic width of the asymmetry distribution being five times larger than the intrinsic width of the acoplanarity, the sensitivity to observe possible energy loss effects is too weak. The measured broadening of the acoplanarity is consistent with dimuon re-scattering with electric charges in the QGP. Details of this analysis and interpretation of the results can be found in Ref. [8].

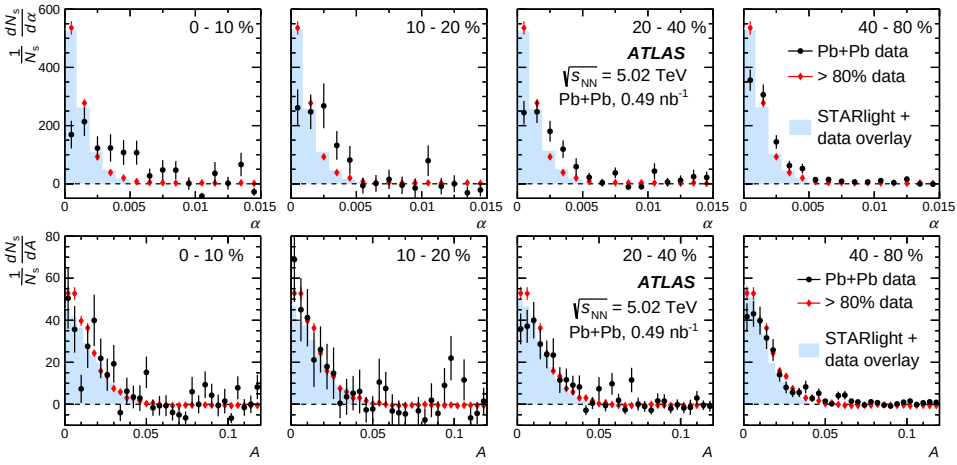

Fig. 3. (Colour on-line) The background-subtracted distributions are shown for α (upper row) and A (lower row). Each distribution is normalized to unity over its measured range. Moving from left to right, data (circles) are shown for increasingly peripheral collisions (lower degree of overlap, higher percentile). The distributions obtained from the MC simulation ($\gamma\gamma \to \mu^{+}\mu^{-}$ generated by STARlight and overlaid on data) are shown for the corresponding centrality interval as a filled histogram. The distribution measured in the most peripheral collisions, the $> 80\%$ interval (diamonds), is repeated in each panel to facilitate a direct comparison. The error bars include statistical and systematic uncertainties. Uncertainties related to background normalization are not shown. See Ref. [8].

5. Jet "quenching"

Jets constitute a golden probe to study the quark–gluon plasma produced in heavy-ion collisions at the LHC. The hard scattered quarks and gluons emerging at the early stages of these collisions evolve as parton showers that propagate through the hot and dense medium. Constituents of the parton showers emit medium-induced gluon radiation and, as a consequence, the resulting jet loses energy, a phenomenon commonly termed as "jet quenching" [10]. Jets produced in heavy-ion collisions are thus expected to be suppressed at a given p_{T}, relatively to a sample produced in pp collisions. The nuclear modification factor R_{AA}, defined as the ratio of normalized yields in Pb+Pb and pp collision systems, is used to compare the inclusive transverse momentum distributions measured in the two collision systems

$$R_{AA} \equiv \frac{(1/N_{\mathrm{evt}})\ \mathrm{d}^2 N_{\mathrm{jet}}^{\mathrm{PbPb}}/\mathrm{d}p_{\mathrm{T}}\mathrm{d}y|_{\mathrm{cent}}}{\langle T_{AA}\rangle \mathrm{d}^2\sigma_{\mathrm{jet}}^{pp}/\mathrm{d}p_{\mathrm{T}}\mathrm{d}y},$$

where $\langle T_{AA}\rangle$ stands for the geometric enhancement of per-collision nucleon–nucleon luminosity and N_{evt} is the total number of Pb+Pb collisions within a chosen centrality interval. The nuclear modification factor R_{AA}, resulting from distributions unfolded for detector resolution, bin-to-bin migration and reconstruction inefficiency, is shown in Fig. 4. Jets are suppressed by a factor of two in central collisions (0–10%), while showing clear dependence on jet transverse momentum [9]. These measurements confirm the expectations on

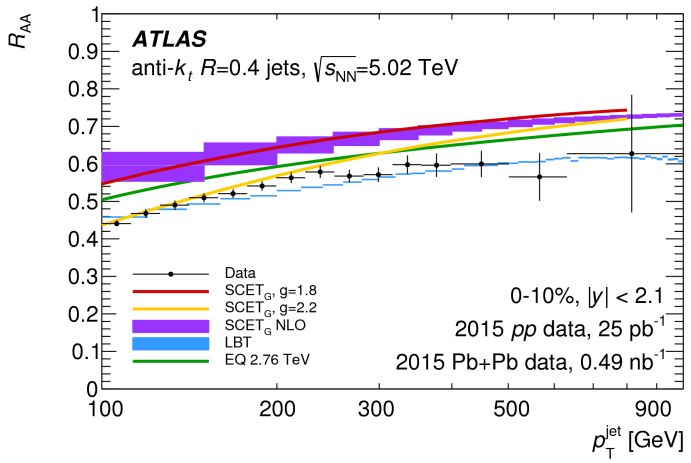

Fig. 4. (Colour on-line) The R_{AA} as a function of jet p_{T} for jets produced in central collisions (0–10%) and with $|y| < 2.1$ compared with theory predictions. The uncertainties of the data points are the combined statistical and systematic uncertainties [9]. The vertical width of the distribution shown for the LBT and SCETG NLO models represents the uncertainty of the theory prediction [11–13].

the reduction of the jet yields at a given transverse momentum due to the interaction of partons in the QGP [10]. The Linear Boltzmann Transport model, that combines kinetic description of parton propagation with hydrodynamic description of the underlying medium evolution, confirms very reasonably both the trend and magnitude of the R_{AA} [11].

The first indication of jet quenching was given by the observation of large asymmetrical dijet events [14, 15]. Dijets probe differences in the two parton showers since in most of the cases the interaction of the two outgoing partons in the QGP is not identical. A new analysis has been performed using the 3 μb^{-1} of Xe+Xe data taken at $\sqrt{s_{NN}} = 5.44$ TeV. The interest of studying jet quenching in Xe+Xe collisions is justified because the underlying event is smaller in the most central collisions. On the other hand, the smaller number of nucleons, or the difference between the nuclear radius of the lead and xenon nuclei, may affect the amount of jet quenching through a reduction in both the overall energy density and the path lengths of the hard-scattered partons in the medium. The analysis involves the two highest-p_{T} jets in the event where the leading jet, or p_{T_1}, is required to be greater than 100 GeV and that of the sub-leading jet, or p_{T_2}, is required to be greater than 35 GeV. Both jets must have $|\eta| < 2.1$. The minimum azimuthal opening angle between the two jets is $\Delta\phi = 7\pi/8$. The comparison between Xe+Xe and 5.02 TeV Pb+Pb dijet distributions as a function of x_{J}, the ratio between the transverse momenta of the two leading jets, is shown in Fig. 5 for the

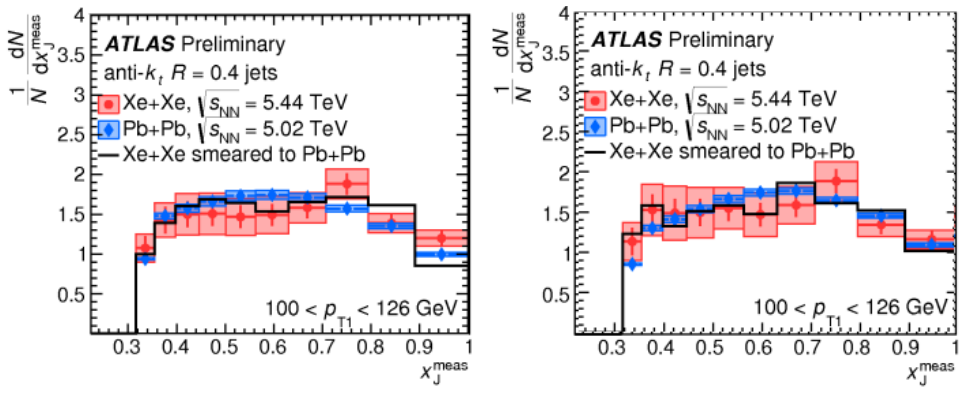

Fig. 5. (Colour on-line) The $(1/N)(\mathrm{d}N/x_{\mathrm{J}}^{\mathrm{meas}})$ distributions for jet pairs with 100 $< p_{\mathrm{T}_1} <$ 126 GeV in the 0–10% centrality interval (left panel) and the range of the transverse energy deposited in the forward calorimeters $2.05 < \sum E_{\mathrm{T}}^{\mathrm{FCal}} < 2.99$ TeV (right panel). The Xe+Xe data are shown in circles, while the Pb+Pb distribution is shown for comparison in diamonds. Statistical uncertainties are indicated by the error bars, while systematic uncertainties are shown with shaded boxes. The black line represents the inclusion of additional fluctuations based on the results of the fluctuations analysis described in [16].

0–10% centrality interval (left panel) and the range of the transverse energy deposited in the forward calorimeters $2.05 < \sum E_{\mathrm{T}}^{\mathrm{FCal}} < 2.99$ TeV (right panel). The former aims at providing a comparison of the geometry and the latter a comparison of the density. The transverse momentum of the leading jet is $100 < p_{\mathrm{T}_1} < 126$ GeV. The observation of large asymmetric dijets is striking. The measured distributions in this preliminary analysis are not unfolded to account for the effects of experimental resolution and inefficiencies on the two-dimensional $(p_{\mathrm{T}_1}, p_{\mathrm{T}_2})$ distributions. The $x_{\mathrm{J}}^{\mathrm{meas}}$ distributions in the two collision systems are consistent within statistical and systematic uncertainties. The black line in the figures shows the effect of the additional smearing applied to the Xe+Xe data using the calorimeter fluctuation analysis described in [16]. The curve shows that the smearing has no impact on the distribution within uncertainties.

6. Quarkonia production

Quarkonia produced in ultra-relativistic heavy-ion collisions is the longer standing puzzle of the Heavy Ion program. A paper written 33 years ago by Matsui and Satz [17] advocated, before any experiment, that an observed suppression of the J/ψ meson would constitute an unambiguous signature of the QGP. The postulate was that when the Debye length becomes smaller than the quarkonium binding radius, the mesons are prevented from forming. This postulate also led to the hypothesis that $\psi(2S)$ would be suppressed before J/ψ. These predictions were soon confirmed experimentally by the NA50 experiment at the CERN SPS [18, 19] ($\sqrt{s_{NN}} = 17.3$ GeV) and later by the PHENIX experiment at BNL RHIC [20] ($\sqrt{s_{NN}} = 200$ GeV). At the LHC energies, the J/ψ meson originates not only from $c\bar{c}$ binding, or feeddown from excited states, but also from b-meson decays, which result in a decay vertex separated from the collision vertex by up to a few millimetres. It is important to disentangle these two production mechanisms because prompt J/ψ production is expected to be sensitive to colour screening and recombination of charm quarks and anti-quarks from the medium in the QGP, whereas non-prompt J/ψ is expected to be sensitive to the energy loss of the b quarks in the QGP. The variable that allows to disentangle the two production mechanisms is the pseudo-proper time, defined as $\tau = L_{xy} m_{\mu\mu}/{p_{\mathrm{T}}}^{\mu\mu}$, where $m_{\mu\mu}$ and ${p_{\mathrm{T}}}^{\mu\mu}$ refer to the mass and transverse momentum of the dimuon decaying pair, and L_{xy} is the distance between the primary and b-meson decay vertices, projected on the transverse plane. Prompt and non-prompt J/ψ and $\psi(2S)$ yields are extracted from two-dimensional unbinned maximum-likelihood fits to the dimuon mass spectrum and pseudo-proper time. The measurement is performed in the dimuon decay channel for $9 < {p_{\mathrm{T}}}^{\mu\mu} < 40$ GeV in dimuon transverse momentum, and

$-2.0 < y^{\mu\mu} < 2.0$ in rapidity. Events were collected using a trigger requiring that the event contains at least two reconstructed muons, each with $p_{\mathrm{T}} > 4$ GeV.

The left panel of Fig. 6 shows the nuclear modification factor, R_{AA}, for prompt J/ψ as a function of the transverse momentum. The plot concerns central Pb+Pb collisions and a strong J/ψ suppression is observed (by a factor of almost 5). The measurement is compared with several models [22–25] advocating colour screening and parton energy loss. All models have tension in describing the whole phase space. The right panel of Fig. 6 shows the prompt $\psi(2S)$ to J/ψ ratio as a function of the number of participants, N_{part}. In such a production mechanism $\psi(2S)$ is more suppressed than J/ψ. The increase of the double R_{AA} ratio in central collisions suggests that $\psi(2S)$ recombines more than J/ψ. Models [24, 26] foresee that $\psi(2S)$ is more suppressed than J/ψ, but fail in describing all centralities simultaneously. Details of this analysis can be found in Ref. [21].

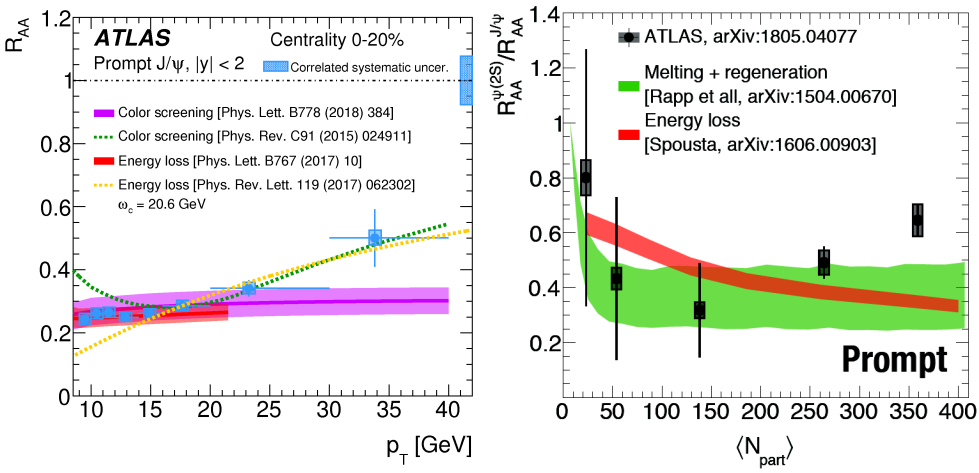

Fig. 6. (Colour on-line) The nuclear modification factor, R_{AA}, for the non-prompt J/ψ meson as a function of p_{T} (left panel) and the $\psi(2S)$ to J/ψ double ratio as a function of the number of participants, N_{part} (right panel). The error bar represents the statistical uncertainties, while the error box represents the total systematic uncertainty. See Ref. [21].

A compilation of results for the nuclear modification factor R_{AA} as a function of p_{T} in different channels and in central Pb+Pb collisions are shown in Fig. 7. The R_{AA} of charged hadrons shows a striking non-flat p_{T} dependence shape. The overall distributions suggest a high-p_{T} universality on the suppression of the different probes. In particular, the result indicates that prompt J/ψ may also be sensitive to parton energy loss [21].

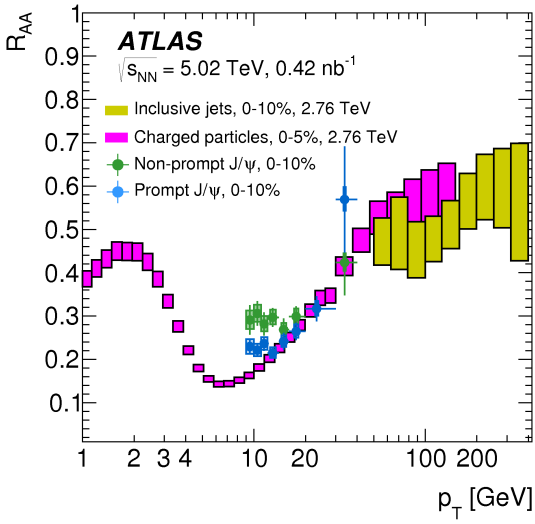

Fig. 7. (Colour on-line) Compilation of results for the nuclear modification factor R_{AA} as a function of p_{T} in different channels from the Run 2 Pb+Pb and pp data. Results are shown for charged hadrons (dark grey/pink), anti-k_{T} $R = 0.4$ jets (light grey/yellow), prompt (medium grey/blue) and non-prompt (black/green) J/ψ. The statistical uncertainties are shown as vertical bars and the total systematic uncertainties, including pp luminosity and $\langle T_{AA} \rangle$ uncertainties, are shown as boxes [21].

7. Conclusions

Data taken by ATLAS at the LHC in Run 2 provided a broad heavy-ion physics program. The ratio of the magnitude of the harmonics flow, v_n, between Xe+Xe and Pb+Pb collisions as a function of centrality is found to be qualitatively consistent with theoretical hydrodynamic predictions. In Pb+Pb collisions, the photon-jet p_{T} balance, $x_{\mathrm{J}\gamma}$, distributions are observed to be modified, both in total yield and in shape, when compared with those in pp collisions. These modifications have a smooth onset as a function of collisions centrality and p_{T}^{γ}. The acoplanarity distributions of muon pair production in Pb+Pb collisions through the process $\gamma\gamma \to \mu^+\mu^-$ are broadened in increasingly central collisions. No such broadening is seen in the asymmetry distributions, where the sensitivity is limited by momentum resolution. Inclusive jet yields are found to be suppressed, reaching a factor of two in central collisions, while showing clear dependence on jet transverse momentum. The raw measurement of the p_{T} balance of dijets produced in Xe+Xe collisions is significantly asymmetric in central collisions and is well in agreement with the respective raw measurement in Pb+Pb collisions. J/ψ production is strongly suppressed in Pb+Pb collisions. Prompt $\psi(2S)$ is

shown to be more suppressed than prompt J/ψ, confirming the long-term expectations associated to step melting pattern, but regenerates in central collisions.

The author thanks the Epiphany 2019 Organizing Committee for the kind invitation to present the above results, and acknowledges the financial support of Fundação para a Ciência e a Tecnologia (FCT) through FCT Researcher contract IF/01586/2014/CP1248/CT0003.

REFERENCES

[1] ATLAS Collaboration, *JINST* **3**, S08003 (2008).

[2] M.L. Miller, K. Reygers, S.J. Sanders, P. Steinberg, *Annu. Rev. Nucl. Part. Sci.* **57**, 205 (2007).

[3] ATLAS Collaboration, *Phys. Lett. B* **707**, 330 (2012) [arXiv:1108.6018 [hep-ex]].

[4] G. Giacalone, J. Noronha-Hostler, M. Luzum, J.-Y. Ollitrault, *Phys. Rev. C* **97**, 034904 (2018) [arXiv:1711.08499 [nucl-th]].

[5] ATLAS Collaboration, ATLAS-CONF-2018-011, https://cds.cern.ch/record/2318870

[6] ATLAS Collaboration, CERN-EP-2018-100, *Phys. Rev. Lett.* **121**, 212301 (2018) [arXiv:1806.08708 [hep-ex]].

[7] S.R. Klein *et al.*, *Comput. Phys. Commun.* **212**, 258 (2017) [arXiv:1607.03838 [hep-ph]].

[8] ATLAS Collaboration, *Phys. Rev. Lett.* **121**, 212301 (2018) [arXiv:1806.08708 [hep-ex]].

[9] ATLAS Collaboration, *Phys. Lett. B* **790**, 108 (2019) [arXiv:1805.05635 [nucl-ex]].

[10] J.-P. Blaizot, Y. Mehtar-Tani, *J. Mod. Phys. E* **24**, 1530012 (2015) and references therein [arXiv:1503.05958 [hep-ph]].

[11] Y. He, T. Luo, X.-N. Wang, Y. Zhu, *Phys. Rev. C* **91**, 054908 (2015) [arXiv:1503.03313 [nucl-th]].

[12] Yang-Ting Chien *et al.*, *Phys. Rev. D* **93**, 074030 (2016) [arXiv:1509.02936 [hep-ph]].

[13] M. Spousta, B. Cole, *Eur. Phys. J. C* **76**, 50 (2016) [arXiv:1504.05169 [hep-ph]].

[14] ATLAS Collaboration, *Phys. Rev. Lett.* **105**, 252303 (2010) [arXiv:1011.6182 [hep-ex]].

[15] ATLAS Collaboration, *Phys. Lett. B* **756**, 10 (2016) [arXiv:1512.00197 [hep-ex]].

[16] ATLAS Collaboration, ATLAS-CONF-2018-007, https://cds.cern.ch/record/2318588

[17] T. Matsui, H. Satz, *Phys. Lett. B* **178**, 416 (1986).

[18] NA50 Collaboration, *Eur. Phys. J. C* **39**, 335 (2005) [arXiv:hep-ex/0412036].

[19] NA50 Collaboration, *Eur. Phys. J. C* **49**, 559 (2007) [arXiv:nucl-ex/0612013].

[20] PHENIX Collaboration, *Phys. Rev. Lett.* **98**, 232301 (2007) [arXiv:nucl-ex/0611020].

[21] ATLAS Collaboration, *Eur. Phys. J. C* **78**, 762 (2018) [arXiv:1805.04077 [nucl-ex]]. Figure 7 at https://atlas.web.cern.ch/Atlas/GROUPS/PHYSICS/PAPERS/HION-2016-07/

[22] S. Aronson, *Phys. Lett. B* **778**, 384 (2018) [arXiv:1709.02372 [hep-ph]].

[23] B.Z. Kopeliovich, I.K. Potashnikova, I. Schmidt, M. Siddikov, *Phys. Rev. C* **91**, 024911 (2015).

[24] M. Spousta, *Phys. Lett. B* **767**, 10 (2017) [arXiv:1606.00903 [hep-ph]].

[25] F. Arleo, *Phys. Rev. Lett.* **119**, 062302 (2017).

[26] X. Du, R. Rapp, *Nucl. Phys. A* **943**, 147 (2015) [arXiv:1504.00670 [hep-ph]].